Interfacial Behaviour in Ferroalloys: The Influence of FeMn Slag Composition

SERGEY BUBLIK, MERETE TANGSTAD, and KRISTIAN ETIENNE EINARSRUD
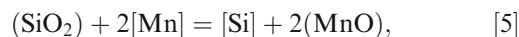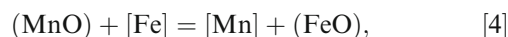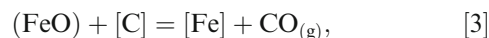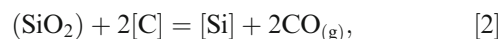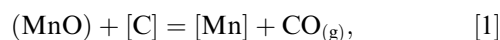
The present study investigated the interfacial interaction between FeMn alloy and slags of different compositions and basicity from 0.4 to 1.2 in a sessile drop furnace. Interfacial tension between the FeMn alloy and the slags was measured, and the results were analyzed to assess the sensitivity of the applied methodology. The measurement of the interfacial tension was based on combining the results from experiments, multiphase flow simulations in OpenFOAM, equilibrium calculations in FactSage, and calculation of slag density and surface tension based on numerical models. The results demonstrate that the interfacial tension between the FeMn alloy and slag increases with the slag basicity. It was found that the addition of Al_2O_3 to the slag with basicity of 0.8 and 1.2 increases the interfacial tension, while increasing MnO content from 30.0 to 45.0 wt pct does not have any statistically significant influence on the interfacial tension. EPMA analysis of slag and FeMn phases showed that slags at lower basicities and the FeMn alloy form a metal–slag emulsion due to the destabilization of the interface induced by chemical reactions, partial reduction of SiO_2 in the slag and the mass transfer of Si across the metal–slag interface.

I. INTRODUCTION

THE carbothermic reduction of manganese ores for producing FeMn alloy in submerged arc furnaces is related to the formation of a significant amount of molten slag, which is then tapped simultaneously with FeMn to ladles, where a metal–slag emulsion is formed. Small FeMn droplets are entrained in the slag phase due to the intensive mixing of FeMn and slag. This decreases efficiency of the ferroalloy production process because further removal of metal from slag may cause logistics difficulties and is heavily time- and energy-consuming.[1,2] Interfacial tension between molten metal and slag characterizes the metal-slag separation[3] and thus it is important for ferroalloy production. High interfacial tension promotes a high degree of separation of metal and slag, while a low interfacial tension will promote formation of metal–slag emulsion and small metal droplets in slag.[4] Several studies have shown that the interfacial tension is greatly dependent upon the slag composition due to chemical reactions at the metal–slag interface and the mass transfer across the interface.[5–12]

In FeMn production, the FeMn alloy is highly saturated with carbon, which results in reduction of oxides such as MnO, FeO or SiO_2 at the interface between FeMn and slag, and subsequently in the mass transfer of Mn, Fe and Si to the FeMn alloy. The thermodynamic equilibrium between ferroalloy and slag can be described by several reduction reactions:[13]

$$(MnO) + [C] = [Mn] + CO_{(g)}, \qquad [1]$$

$$(SiO_2) + 2[C] = [Si] + 2CO_{(g)}, \qquad [2]$$

$$(FeO) + [C] = [Fe] + CO_{(g)}, \qquad [3]$$

$$(MnO) + [Fe] = [Mn] + (FeO), \qquad [4]$$

$$(SiO_2) + 2[Mn] = [Si] + 2(MnO), \qquad [5]$$

where [] and () denote chemical constituents in the FeMn alloy and the slag, respectively.

The determination of the metal–slag interfacial tension is challenging as it requires applying high temperatures and recording metal–slag interaction with X-ray imaging[14] or a digital camera.[6] Generally, these methods may have significant experimental uncertainty

SERGEY BUBLIK, MERETE TANGSTAD, and KRISTIAN ETIENNE EINARSRUD are with the Department of Materials Science and Engineering, Norwegian University of Science and Technology (NTNU), 7491 Trondheim, Norway. Contact e-mail: sergey.bublik@ntnu.no

due to sensitivity to impurities present in raw materials and crucibles, or the resolution of X-ray images.[15] Therefore, the use of advanced analysis and modelling tools can be of great help in understanding the interfacial phenomena and in improving and simplifying the experimental setup for measuring interfacial tension.

In the current study, the interfacial interaction between FeMn alloy and slags of different compositions was investigated in a sessile drop furnace using the methodology developed by the authors previously,[16,17] which was improved in this study to improve reproducibility and reduce uncertainty due to the precipitation of solid carbon during melting of FeMn alloy and slag. The improved methodology combines analysis of images from experiments in the sessile drop furnace, numerical data obtained in multiphase flow simulations in OpenFOAM v8,[18] the numerical models for calculation of density and surface tension of slag developed by Mills *et al.*[19,20] and results of equilibrium calculations in FactSage 7.3.[21] In addition, the sensitivity of the results was assessed by comparing different experiments.

II. EXPERIMENTAL

A. *Material Preparation*

Synthetic FeMn alloy and slags have been prepared from pure powders for studying interfacial tension in the sessile drop furnace. Compositions of the FeMn alloy and the slags have been selected based on the composition of industrial materials and, in addition, the synthetic slags have been selected to cover the most relevant slags for FeMn production. The calculated composition of the synthetic raw materials and the purity of powders used for material preparation are specified in Tables IV and V in "Appendix A", respectively. The composition of FeMn alloy and slag measured by the X-ray fluorescence (XRF) and the combustion infrared detection (combustion-IR) techniques is shown in Table I. The corresponding normalized data is given in Table VI in "Appendix A".

The powders were mixed and melted separately in graphite crucibles in an induction furnace in Ar atmosphere at temperature of 1773 K and holding time of 60 minutes for the FeMn alloy and 5 minutes for master slags. After the first melting, the FeMn alloy and the master slags were cooled down in the crucibles and ground in a ball mill. Thereafter, the master slags were divided into batches of 20 g and an additional amount of the oxide powders has been added according to the composition of the final slags. Both the FeMn alloy and the master slags were then remelted using the same operational parameters in the induction furnace. The amount of the powders required to produce the synthetic materials has been calculated taking into account the purity of the powders and the composition of the industrial materials[1] and is presented in Table VII in "Appendix A". Note that carbon has not been added as a raw material for melting of the FeMn alloy as it is

contained in the graphite crucible—this allows to saturate the required amount of carbon, ≈ 7 wt pct for the FeMn alloy.

B. *Experimental Setup*

A sessile drop furnace (Figure 1) has been applied for investigating the interfacial interaction between the FeMn alloy and the slags as shown in Figure 2. The sessile drop furnace was equipped with a pyrometer and a C-type thermocouple for measuring temperature, and with a digital video camera (Allied Vision Prosilica GT2000, Edmund Optics, Inc., Barrington) with a telecentric lens (Navitar 1-50993D) for recording images of molten samples with the resolution of 2048×1088 pixels at one frame per second after reaching melting temperature of the FeMn alloy and the slags. Every 10 to 15 experiments, the thermocouple was calibrated by melting pure Fe in Ar and assessing its melting temperature from recorded images. The experiments were performed using graphite cups in Ar atmosphere (6N grade) at temperature of 1673 K and holding time of 5 minutes in sets, where three parallels were performed for each slag composition. The heating rate was 300 K/min up to 1473 K and approximately 25 K/min from 1473 K to 1673 K. The graphite cups were cleaned before the experiments with a paper towel dipped in ethanol or acetone and then dried using compressed air. A schematic representation of the slag and the FeMn alloy in the graphite cup before and during the experiments is shown in Figure 3.

After the experiments, the FeMn alloy and the slags were cast in epoxy, sectioned in the centre of the slag droplet, re-cast into epoxy, polished and coated with carbon prior to analysis in EOL JXA-8500F Electron Probe Micro Analyzer (EPMA). The composition of FeMn and slag phases were measured in several points, and the average composition of each phase was calculated based on this. Additionally, the chemical composition of the synthetic FeMn alloy and the slags before the experiments was determined by XRF and combustion-IR. The FeMn alloy was analyzed for Mn, Fe, Si and C, and the slags were analyzed for MnO, CaO, MgO, SiO_2, Al_2O_3 and FeO.

C. *Methodology for Determination of Interfacial Tension*

The methodology for determination of the interfacial tension is based on a comparison of geometrical features obtained from multiphase CFD simulations and the experiments in the sessile drop furnace[17] as illustrated in Figure 4. This methodology was developed by the authors previously[16,17] and has been modified in this paper to improve reproducibility and reduce uncertainty due to the precipitation of solid carbon on the surface of FeMn and slag during the experiments in the sessile drop furnace.

The experimental step is performed to obtain images of slag and metal interaction in the molten state. Here, a set of three individual experiments with the slag droplet placed on top of the FeMn layer in the graphite cup are conducted for each slag composition.

Table I. The Measured Chemical Composition of the Synthetic FeMn Alloy and Slags

Material	Mn	Fe	Si	C	MnO	CaO	MgO	SiO$_2$	Al$_2$O$_3$	FeO	Total	Basicity*
FeMn Alloy	77.30	14.50	0.11	7.52	—	—	—	—	—	—	99.43	—
Slags with Al$_2$O$_3$ Addition												
Slag A1	—	—	—	—	30.62	14.23	6.77	39.52	10.23	0.89	102.26	0.42
Slag A2	—	—	—	—	29.30	25.50	6.75	29.18	10.17	0.79	101.69	0.82
Slag A3	—	—	—	—	28.91	32.00	6.64	22.14	10.19	0.79	100.67	1.20
Slag B1	—	—	—	—	37.90	12.87	6.72	34.15	10.18	0.77	102.59	0.44
Slag B2	—	—	—	—	36.77	22.50	6.58	25.21	10.08	0.74	101.88	0.82
Slag B3	—	—	—	—	37.53	27.87	6.83	18.33	10.01	0.74	101.31	1.22
Slag C1	—	—	—	—	45.43	10.76	6.61	28.84	10.23	0.73	102.60	0.44
Slag C2	—	—	—	—	44.65	19.04	6.83	20.80	10.19	0.73	102.24	0.83
Slag C3	—	—	—	—	45.39	23.92	6.70	15.04	10.01	0.72	101.78	1.22
Slags Without Al$_2$O$_3$ Addition												
Slag D1	—	—	—	—	30.67	14.76	6.10	48.83	0.67	0.89	101.92	0.42
Slag D2	—	—	—	—	29.83	25.30	6.31	38.32	0.77	0.85	101.38	0.81
Slag D3	—	—	—	—	29.27	31.91	6.18	32.23	0.61	0.80	101.00	1.16
Slag E1	—	—	—	—	38.68	12.93	6.09	43.32	0.58	0.77	102.37	0.43
Slag E2	—	—	—	—	37.01	22.69	6.16	34.40	0.69	0.75	101.70	0.82
Slag E3	—	—	—	—	37.24	28.17	6.10	28.36	0.68	0.61	101.16	1.18
Slag F1	—	—	—	—	46.00	10.58	6.23	38.14	0.69	0.71	102.35	0.43
Slag F2	—	—	—	—	44.33	19.64	6.10	30.53	0.56	0.68	101.84	0.83
Slag F3	—	—	—	—	45.33	24.53	6.01	25.02	0.47	0.70	102.06	1.20

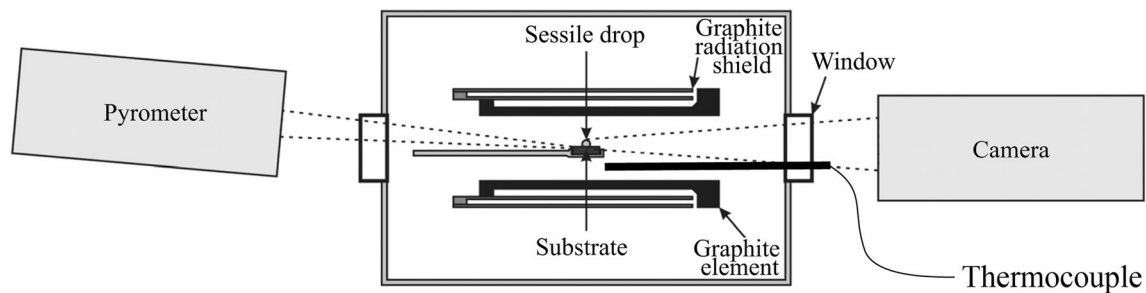*Basicity $(B) = \dfrac{CaO+MgO}{SiO_2+Al_2O_3}$, calculated on mass basis.

Fig. 1—Schematic of the sessile drop furnace. Reprinted from Ref. [22] under the terms of the Creative Commons CC BY license.
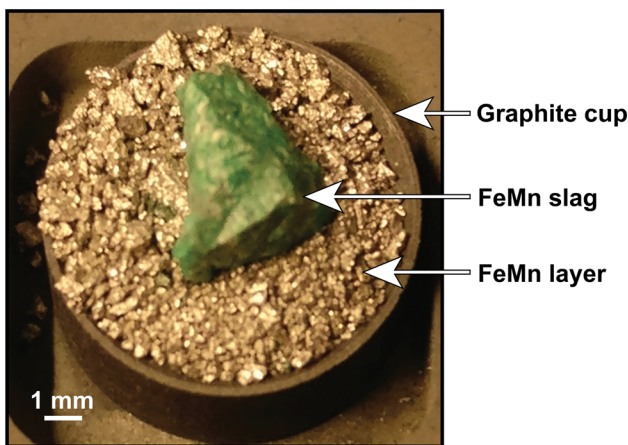

Fig. 2—FeMn alloy and slag in the graphite cup before the experiments in the sessile drop furnace. Reprinted from Ref. [17].

The composition of the slag and metal changes during the experiments, and therefore the composition of the liquid slag and the formed solid monoxide phase must be taken into account to address the change in composition. The amount and composition of liquid slag phase is determined at the adjustment step, which is then used to estimate surface tension and density of the slag droplet at the equilibrium using numerical models developed by Mills et al. [19,20] The adjustment step is performed as follows:

(a) Calculate amount and composition of the liquid slag and solid phases after interaction with the FeMn alloy at 1673 K in FactSage in the equilibrium module using FactPS, FToxid and FTmisc databases.
(b) Calculate the surface tension and the density of the slag droplet and its liquid slag phase using the numerical models developed by Mills et al.
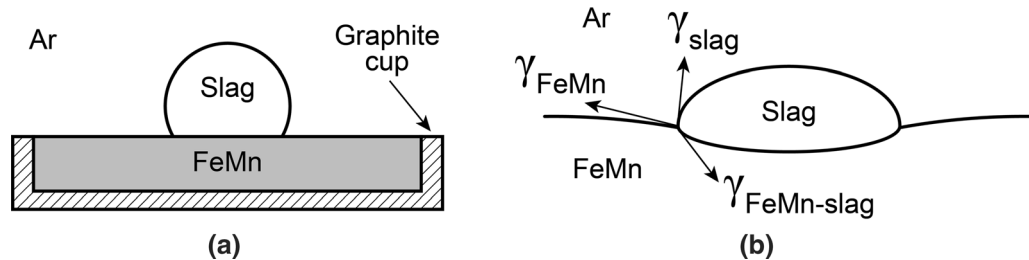
Fig. 3—(a) Schematic cross section of the slag droplet on top of the FeMn alloy in the graphite cup before the experiments. (b) The force balance at the contact point of Ar, slag and FeMn during the experiments. γ_{FeMn} is surface tension of FeMn, γ_{slag} is surface tension of slag, $\gamma_{FeMn-slag}$ is interfacial tension between FeMn and slag. It should be observed that the slag droplet is small compared to the surface of FeMn, ensuring that it does not come in contact with the graphite cup.
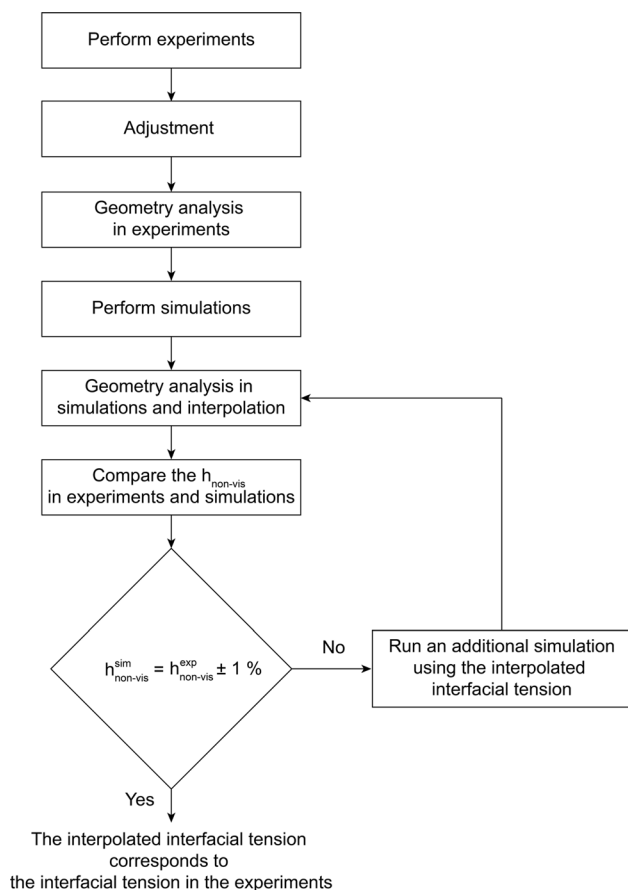

Fig. 4—Schematic describing steps for the determination of interfacial tension in the experiments based on the geometrical parameters of the slag droplet.

(c) Calculate the average surface tension and the average density which can be found as the average between the slag droplet and its liquid phase.

Then, a geometric analysis of the slag droplet in the experiments is carried out to characterize the interfacial interaction between the FeMn alloy and the slags and measure geometrical parameters of the slag droplet. These are assessed after 2 minutes of holding time at the minimum volume expansion of the slag droplet to minimize the influence of volume fluctuations due to chemical reactions and gas evolution on experimental

results. In addition, the surface roughness due to the formation of solid carbon and the amount of FeMn layer filling the graphite cup are addressed. The following substeps are conducted at this step:

(a) Determine the surface correction coefficient for each experiment, k_R, by direct measurement and averaging of the size of particles at the interfaces. In this study, k_R was up to 0.7 mm, depending on the surface roughness, which corresponds to 25 pct of the typical droplet size.

(b) Calculate total volume of the slag droplet, V_{total}, using slag density in the molten state and weight of the slag droplet measured before the experiments:

$$V_{total} = \frac{m_{slag}}{\rho_{slag}}, \qquad [6]$$

where m_{slag} is the weight of the slag droplet.

(c) Calculate visible volume of the slag droplet in the experiments, V_{vis}^{exp}, assuming that the slag droplet forms a spherical cap both above and below the FeMn–gas interface and subtracting k_R from visible height and radius of the slag droplet:

$$V_{vis}^{exp} = \frac{1}{6}\pi(h_{vis}^{exp} - k_R)(3(a^{exp} - k_R)^2 + (h_{vis}^{exp} - k_R)^2),$$

$$[7]$$

where h_{vis}^{exp} is the visible height of the slag droplet and a^{exp} is the measured radius of the slag droplet.

(d) Calculate non-visible volume of the slag droplet in the experiments, $V_{non-vis}^{exp}$:

$$V_{non-vis}^{exp} = V_{total}^{exp} - V_{vis}^{exp}. \qquad [8]$$

(e) Calculate non-visible height of the slag droplet in the experiments, $h_{non-vis}^{exp}$, by expressing it from the equation:

$$V_{non-vis}^{exp} = \frac{1}{6}\pi h_{non-vis}^{exp}(3(a^{exp} - k_R)^2 + (h_{non-vis}^{exp})^2). \qquad [9]$$

(f) The FeMn layer does not completely fill the graphite cup, therefore, distance from the FeMn–gas interface to the edge of the graphite cup has to be taken into account as well. It can be calculated using volume of the cup, density of the FeMn alloy in the molten state and weight of the FeMn layer:

$$V_{cup} = \pi r_{cup}^2 h_{cup},\qquad[10]$$

$$V_{FeMn} = \frac{m_{FeMn}}{\rho_{FeMn}},\qquad[11]$$

$$h_{add} = \frac{V_{cup} - V_{FeMn}}{\pi r_{cup}^2},\qquad[12]$$

where V_{cup} is the volume of the cup, r_{cup} is the inner radius of the cup (4 mm), h_{cup} is the inner height of the cup (3 mm), V_{FeMn} is the volume of the FeMn layer, m_{FeMn} is the weight of the FeMn layer, ρ_{FeMn} is the density of FeMn in the molten state (5612 kg/m^3[23]), h_{add} is the distance from the FeMn–gas interface to the edge of the graphite cup, correcting for the cup not being 100 pct filled. A visual explanation of all geometrical parameters is shown in Figure 5.

(g) Considering h_{add}, calculate the non-visible height of the slag droplet in the experiments (in pct):

$$h_{non-vis}^{exp}(pct) = \frac{h_{non-vis}^{exp} - h_{add}}{h_{non-vis}^{exp} + h_{vis}^{exp}} \cdot 100.\qquad[13]$$

(h) Calculate the average non-visible height for each experiment:

$$\overline{h}_{non-vis}^{exp}(pct) = \frac{\sum h_{non-vis}^{exp}(pct)}{n},\qquad[14]$$

where n is the number of observations, considering the minimum volume expansion of the slag droplet.

Furthermore, at the modelling step, simulations are performed using the physical properties and parameters from the experiments: surface tension (assumed to be a constant value of 1.50 N/m as was calculated previously[24] by the authors for the FeMn alloy composition considered in this study) and the density of the FeMn alloy in the molten state; the average surface tension and the average density of slag in the molten state; the weight of the slag droplet and the FeMn layer. As shown in Figure 6, the interfacial interaction between the FeMn alloy and the slag droplet is simulated without walls of the graphite cup. However, the geometrical features of the slag droplet have to be calculated considering that a part of the slag droplet cannot be seen due to the walls. The non-visible height in the simulation is then compared to the non-visible height in the experiment, and if they differ significantly, a new simulation is started. Here, the following substeps are performed:

(a) Perform three parallel simulations using the interfacial tension between the FeMn alloy and the slag droplet of 0.30, 1.15 and 2.00 N/m.
(b) Knowing the apex position of the slag droplet on Y-axis ($Y_{slag\,apex}$) and the edge position of the graphite cup on Y-axis (Y_{edge}), visible height of the slag droplet in simulations can be obtained:

$$h_{vis}^{sim} = Y_{slag\,apex} - Y_{edge},\qquad[15]$$

$$h_{vis}^{sim}(pct) = \frac{h_{vis}^{sim}}{h_{droplet}^{sim}} \cdot 100.\qquad[16]$$

(c) Non-visible height is then expressed as:

$$h_{non-vis}^{sim}(pct) = 100 - h_{vis}^{sim}(pct).\qquad[17]$$
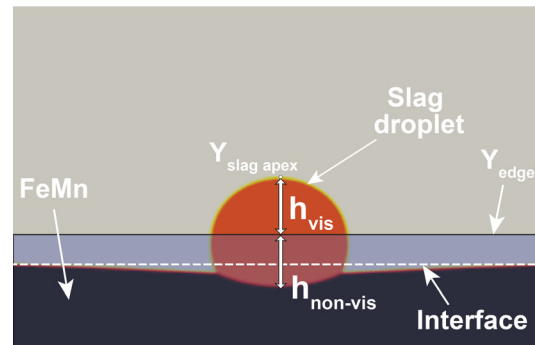
Fig. 6—The slag droplet at the FeMn–Ar interface in the steady state in the simulations. The semi-transparent blue filled area represents the walls of the graphite cup with r_{cup} of 4 mm and h_{cup} of 3 mm (Color figure online).

Fig. 5—Geometrical parameters of the slag droplet (a) and the real position of the interface (b) used in the calculations. Note that the lines shown in the figures are schematic only and may not represent actual measured geometrical parameters.

Consequently, the average non-visible height of the slag droplet in a steady state is calculated (in pct):

$$\overline{h}_{\text{non-vis}}^{\text{sim}}(\text{pct}) = \frac{\sum h_{\text{non-vis}}^{\text{sim}}(\text{pct})}{n_t}, \qquad [18]$$

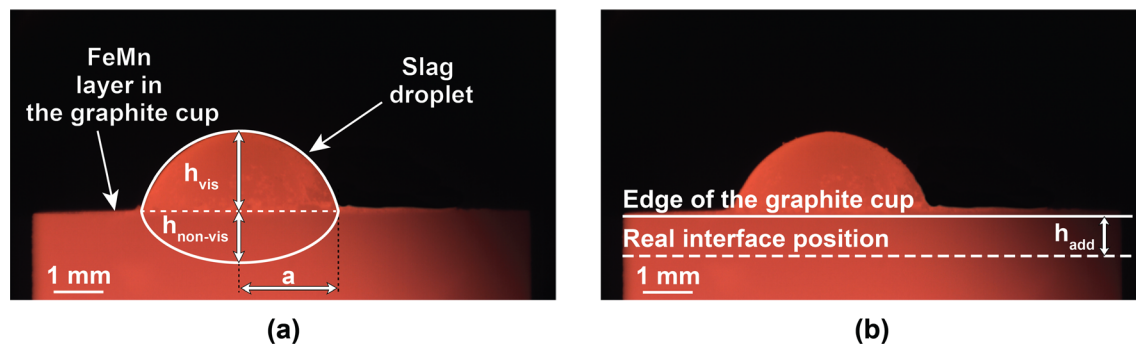where n_t is the number of time steps in the steady state corresponding to the last 0.4 seconds of the simulation. $h_{\text{non-vis}}^{\text{sim}}$ is calculated for each time step and the simulation is stopped when two conditions are met: simulation time is higher than 0.8 seconds and $\overline{h}_{\text{non-vis}}^{\text{sim}}(\text{pct})$ is almost constant (± 2 pct) during the last 0.4 seconds of the simulation, i.e., when the steady state is reached.

(d) Linearly interpolate $\overline{h}_{\text{non-vis}}^{\text{sim}}(\text{pct})$ from the current set of simulations as a function of the interfacial tension and determine the corresponding value of the interfacial tension to $\overline{h}_{\text{non-vis}}^{\text{exp}}$.

(e) Perform a simulation using the interpolated interfacial tension and calculate $\overline{h}_{\text{non-vis}}^{\text{sim}}(\text{pct})$ as described in step (c).

(f) Repeat steps from (c) to (e) until $\overline{h}_{\text{non-vis}}^{\text{sim}}(\text{pct})$ is ± 1 pct from the experimental value ($\overline{h}_{\text{non-vis}}^{\text{exp}}$).

The 80 pct confidence interval was calculated for each set of three experiments based on the Student's t-distribution[25]:

$$\text{CI} = \overline{y} \pm t \frac{s}{\sqrt{n}}, \qquad [19]$$

where $\overline{y}$ is the sample mean, t is the critical value found from the confidence level and degrees of freedom of the sample (1.886 for a two-tailed test with a statistical significance of 0.2 and two degrees of freedom), s is the sample standard deviation and n is the number of experiments in a set. Here, s is expressed as:

$$s = \sqrt{\frac{\sum_{i=1}^{n}(y_i - \overline{y})^2}{n-1}}, \qquad [20]$$

where $y_i \{y_1, y_2, \ldots, y_n\}$ represents one measured value of the sample (i.e., interfacial tension in a single experiment).

III. RESULTS AND DISCUSSION

A. Surface Tension and Density of Slags

The composition of liquid slag phase of the slags after interaction with the FeMn alloy at 1673 K was calculated in FactSage and is shown in Table II. As can be seen from this table, the composition of the liquid slag changes after reacting with FeMn, which can be partially attributed to the reduction of MnO to Mn by Reaction (1) and mainly due to the formation of solid MnO–MgO–CaO phase resulting in a lower MnO and MgO content in the liquid slag when the basicity increases. In addition, there is no solid slag phase at low slag basicity of 0.4 and SiO_2 in the slag is partially

reduced to the metal phase by Reaction (2). Note that Al_2O_3 remains in the liquid slag phase and FeO introduced into the slag by impurities in the raw materials is completely reduced to the metal phase through Reaction (3).

The surface tension and density of the slags, as given in Table III, were calculated considering the composition of the initial slag (Table I) and the liquid slag phase calculated in FactSage. The surface tension does not vary significantly between the initial slag and the liquid slag phase; the maximum variation of 0.025 N/m (5.5 pct) was observed for slag D1. Higher values of the surface tension at higher basicities are related to the composition change, thereby the content of CaO increases while SiO_2 decreases. CaO has a high surface tension of 0.625 N/m in its pure form, whereas surface tension of pure SiO_2 (0.260 N/m) is substantially lower.[20] In addition, slags without Al_2O_3 addition have lower surface tension due to the low content of Al_2O_3 which has a high surface tension of 0.655 N/m. However, the variation in the density between the initial slag and the liquid slag phase is higher and reaches 301 kg/m^3 or 9.6 pct for slag C3. The density for the initial slags is almost constant regardless of the slag basicity, but it increases when MnO and Al_2O_3 content in the slags increases as they have a higher density of 5370 and 3965 kg/m^3, respectively, in their pure form compared with CaO (3340 kg/m^3), MgO (3580 kg/m^3) and SiO_2 (2650 kg/m^3).[26] For the liquid slag phase, the density decreases with the slag basicity due to the significant change in the composition of the liquid phase after interacting with the FeMn alloy, which leads to a lower MnO content.

B. Effect of Slag Composition on Interfacial Tension

The interfacial tension between the FeMn alloy and the slags with and without Al_2O_3 addition is shown in Figures 7 and 8, respectively. It can be seen from the figures that the interfacial tension sharply increases with the slag basicity for both groups of slags. Moreover, for slags with Al_2O_3, the increase in interfacial tension is more pronounceable at higher basicities. As such, the average interfacial tension for the slags with Al_2O_3 addition is 0.21 to 0.40 N/m higher at the basicity of 0.8, and 0.05 to 0.36 N/m higher for the basicity of 1.2. In addition, the 80 pct confidence intervals overlap greatly in each group of basicities due to the low number of experiments in parallels; however, the measured values of the interfacial tension fall within the proposed ranges of the confidence intervals. Increasing MnO content in slag from 30.0 to 45.0 wt pct does not show statistically significant differences in the interfacial tension for all slags. Here, it is important to note that due to the fluctuations of the slag droplet during reaction with the FeMn alloy, which can influence the experimental results, the non-visible height and, accordingly, the interfacial tension were measured only at local minimum expansion of the slag droplet as shown in Figure 9.

Table II. The Chemical Composition of the Liquid Slag Phase After Interaction with the FeMn Alloy Calculated in FactSage

Liquid Phase Corresponding to	Chemical Composition (Wt Pct)				
	MnO	CaO	MgO	SiO_2	Al_2O_3
Slags with Al_2O_3 Addition					
Slag A1	34.76	14.05	6.68	34.41	10.10
Slag A2	26.60	26.22	6.95	29.72	10.46
Slag A3	21.15	36.27	4.92	25.57	12.11
Slag B1	38.15	12.96	6.77	31.87	10.25
Slag B2	31.42	24.09	6.68	27.02	10.79
Slag B3	22.82	35.91	3.92	24.26	13.09
Slag C1	42.75	11.11	6.82	28.75	10.56
Slag C2	33.28	23.20	5.52	25.53	12.46
Slag C3	24.77	34.36	3.33	22.70	14.83
Slags Without Al_2O_3 Addition					
Slag D1	42.66	13.56	5.60	37.55	0.62
Slag D2	31.69	25.55	6.37	35.61	0.78
Slag D3	26.18	33.26	6.51	33.39	0.65
Slag E1	44.43	12.76	6.01	36.22	0.58
Slag E2	35.92	23.33	6.34	33.70	0.71
Slag E3	29.87	31.51	6.14	31.72	0.76
Slag F1	48.34	10.65	6.28	34.03	0.69
Slag F2	40.96	20.64	6.41	31.41	0.59
Slag F3	31.82	30.69	5.47	31.42	0.59

Table III. The Calculated Surface Tension and Density of the Initial Slag and the Liquid Slag Phase

Slag	Surface Tension (N/m)			Density (kg/m^3)		
	Initial Slag	Liquid Phase	Average	Initial Slag	Liquid Phase	Average
Slags with Al_2O_3 Addition						
A1	0.460	0.472	0.466	3138	3223	3181
A2	0.502	0.501	0.502	3170	3126	3148
A3	0.529	0.521	0.525	3187	3076	3132
B1	0.474	0.485	0.479	3270	3313	3292
B2	0.510	0.506	0.508	3292	3209	3251
B3	0.536	0.524	0.530	3318	3108	3213
C1	0.486	0.486	0.486	3414	3376	3395
C2	0.519	0.508	0.514	3426	3247	3337
C3	0.541	0.527	0.534	3446	3145	3296
Slags Without Al_2O_3 Addition						
D1	0.429	0.454	0.442	3025	3266	3146
D2	0.470	0.476	0.473	3083	3115	3099
D3	0.493	0.491	0.492	3103	3050	3077
E1	0.441	0.458	0.450	3169	3298	3234
E2	0.477	0.478	0.478	3201	3185	3193
E3	0.499	0.493	0.496	3229	3110	3170
F1	0.453	0.462	0.458	3311	3375	3343
F2	0.484	0.482	0.483	3327	3270	3299
F3	0.505	0.492	0.499	3360	3139	3250

Previous studies[5,8,27] investigated the mechanisms of the interfacial interaction between molten Fe and CaO–SiO_2–Al_2O_3 slag, where it was suggested that the interfacial tension between slag and metal changes due to reduction or oxidation reactions in molten Fe containing Al (Eq. [21]) or decomposition and dissolution of SiO_2 into molten Fe without Al (Eq. [22]). The interfacial tension rapidly decreases due to the proposed reactions, and then gradually increases before reaching a constant value at the equilibrium between slag and metal. As shown in Figure 9, the similar behaviour can be observed in the current study, when the visible surface area of slag B1 and B2 sharply changes in the beginning of the holding period (0 to 1.5 minutes) and then remains practically constant. This may indicate that the dynamic interfacial oxygen potential and the
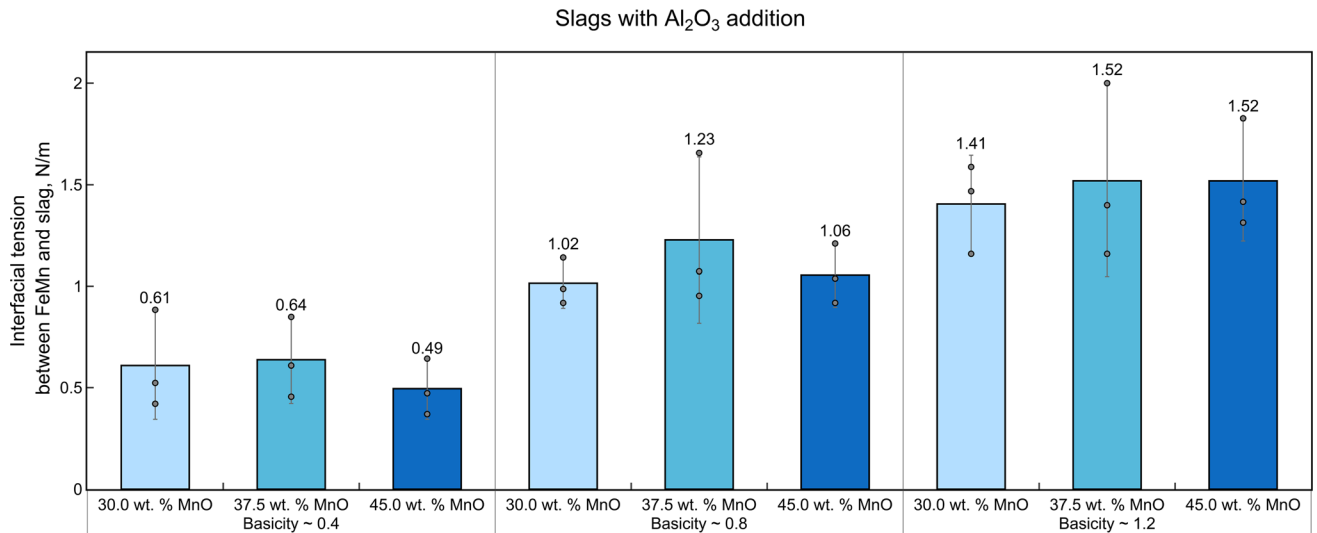
Fig. 7—The interfacial tension between the FeMn alloy and the slag with the addition of Al₂O₃ at different slag basicities and MnO content at 1673 K. The top part of the bars corresponds to the average interfacial tension between the FeMn alloy and the slag. The grey lines on top of bars represent the 80 pct confidence interval, and the circle markers represent the experimental measurements.
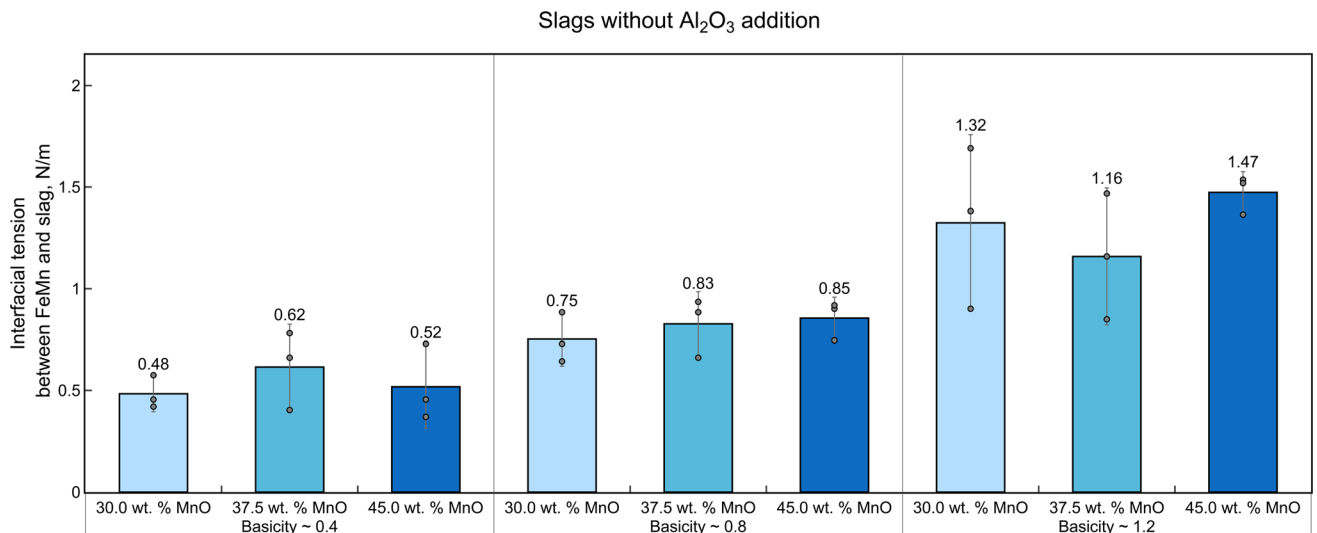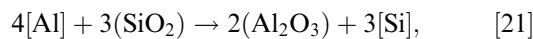

Fig. 8—The interfacial tension between the FeMn alloy and the slag without the addition of Al₂O₃ at different slag basicities and MnO content at 1673 K. The top part of the bars corresponds to the average interfacial tension between the FeMn alloy and the slag. The grey lines on top of bars represent the 80 pct confidence interval, and the circle markers represent the experimental measurements.

mass transfer rate across the interface decrease as reactions between slag and metal proceed as previously was found by Gu *et al.*[28]

$$4[Al] + 3(SiO_2) \rightarrow 2(Al_2O_3) + 3[Si], \quad [21]$$

$$(SiO_2) \rightarrow [Si] + 2[O]. \quad [22]$$

Nakashima and Mori[11] studied interfacial interaction between molten Fe and CaO–SiO₂–Al₂O₃, and CaO–MgO–Al₂O₃ slags, where it was concluded that the interfacial tension can be greatly modified due to the change of slag composition. Several researchers[10,29–31] have shown that a decrease of SiO₂ in slag with increasing CaO/SiO₂ ratio decreases oxygen

content and therefore oxygen activity in molten Fe, which causes an increase of the interfacial tension.[6,7] As such, the addition of CaO and Al₂O₃ to the slag slightly increases the interfacial tension, while the addition of MnO and FeO substantially decreases it. However, it was pointed out that the interfacial tension, depending on MnO content, decreases exponentially, reaching a steady value at high MnO content (after adding 20 mol pct MnO). As it is shown in the present results, the interfacial tension does not change with the MnO content, meaning that a steady value has been reached, after which the interfacial tension does not change after the addition of MnO. The Al₂O₃ addition and the slag basicity also show a similar effect on the interfacial tension, similar to what was reported in the literature.

Interfacial interaction of the slag droplet with the FeMn alloy in the graphite cup depending on different slag composition is shown in Figures 10, 11 and 12. The non-visible height of the slag droplet with MnO content of 30 wt pct decreases with the basicity (Figure 10), which means that the droplet tends to stay at the interface and leads to better separation of slag and metal. Furthermore, the angle between the tangent of the droplet and the top of the crucible θ_{s-cr} increases from 73.8 to 90.4 deg, indicating a reduced contact area between slag and metal owing to increased interfacial tension between these phases.
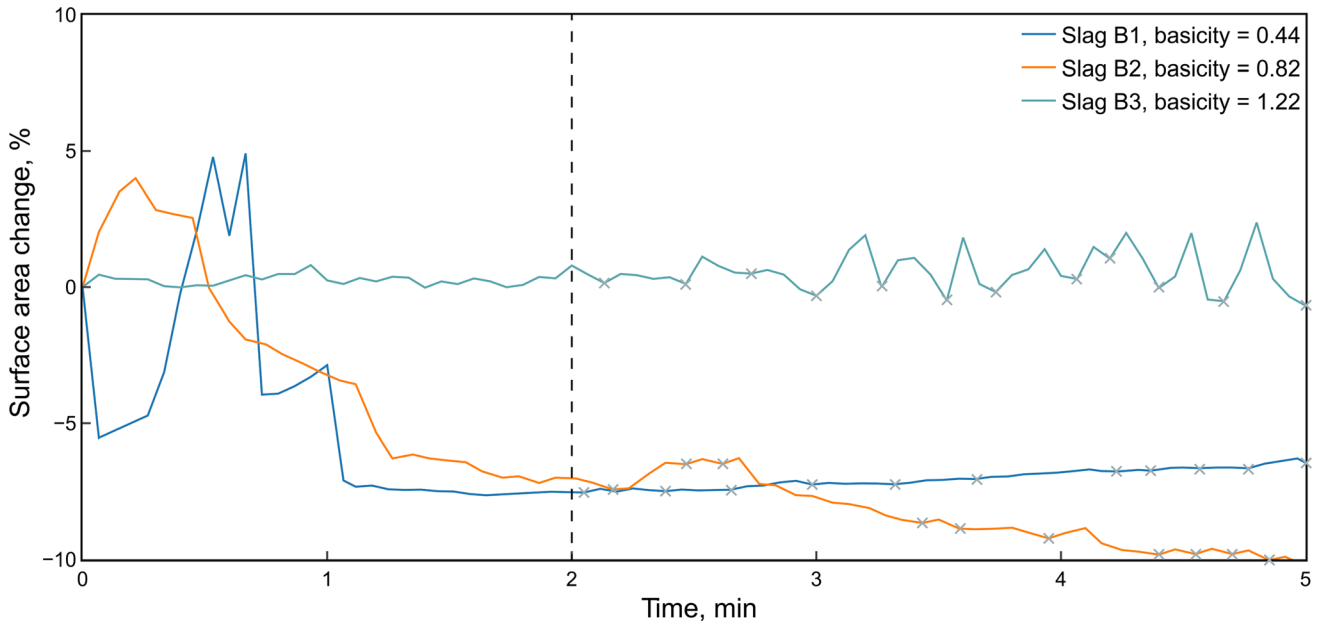
Fig. 9—Temporal change in visible surface area for slags B1–B3 during holding at 1673 K. The grey cross markers correspond to the local minimum expansion of the slag droplet in the experiments. Note that interfacial tension was measured only after 2 minutes of holding time as indicated with the vertical dashed line.

Fig. 10—Slag droplets with various basicity and constant MnO content of 30 wt pct during interaction with the FeMn alloy at 1673 K: (a) slag A1, (b) slag A2, and (c) slag A3. The droplet contour and the real position of the interface are shown by the solid and the dashed line, respectively.
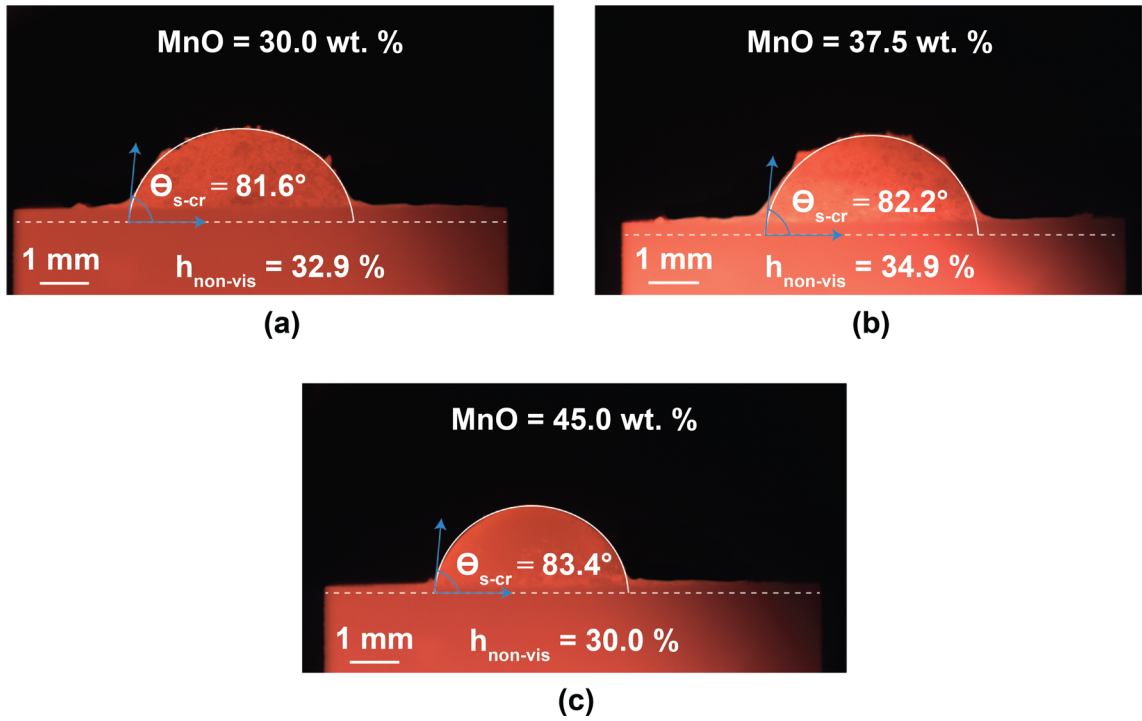
Fig. 11—Slag droplets with constant basicity of 0.8 and various MnO content during interaction with the FeMn alloy at 1673 K: (*a*) slag A2, (*b*) slag B2, and (*c*) slag C2. The droplet contour and the real position of the interface are shown by the solid and the dashed line, respectively.

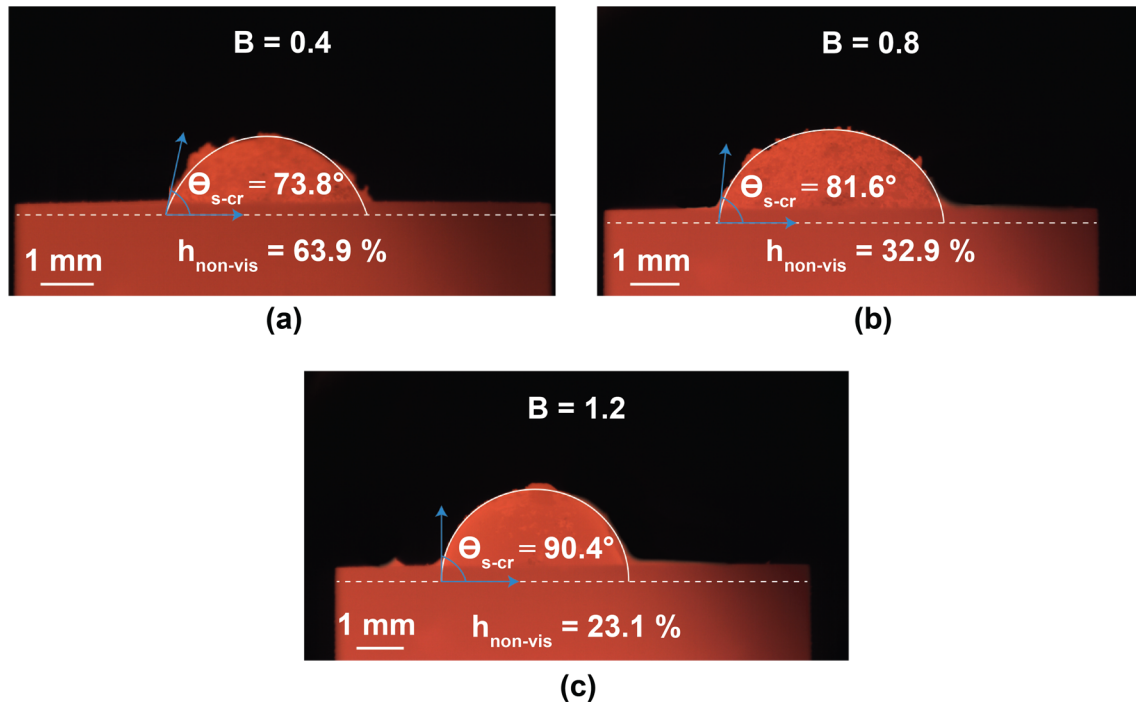Fig. 12—Slag droplets with various basicity and constant MnO content of 37.5 wt pct during interaction with the FeMn alloy at 1673 K. Images (*a*) and (*c*) correspond to slags B1 and B2 (with Al_2O_3 addition); images (*b*) and (*d*) show slags E1 and E2 (without Al_2O_3 addition). The droplet contour and the real position of the interface are shown by the solid and the dashed line, respectively.

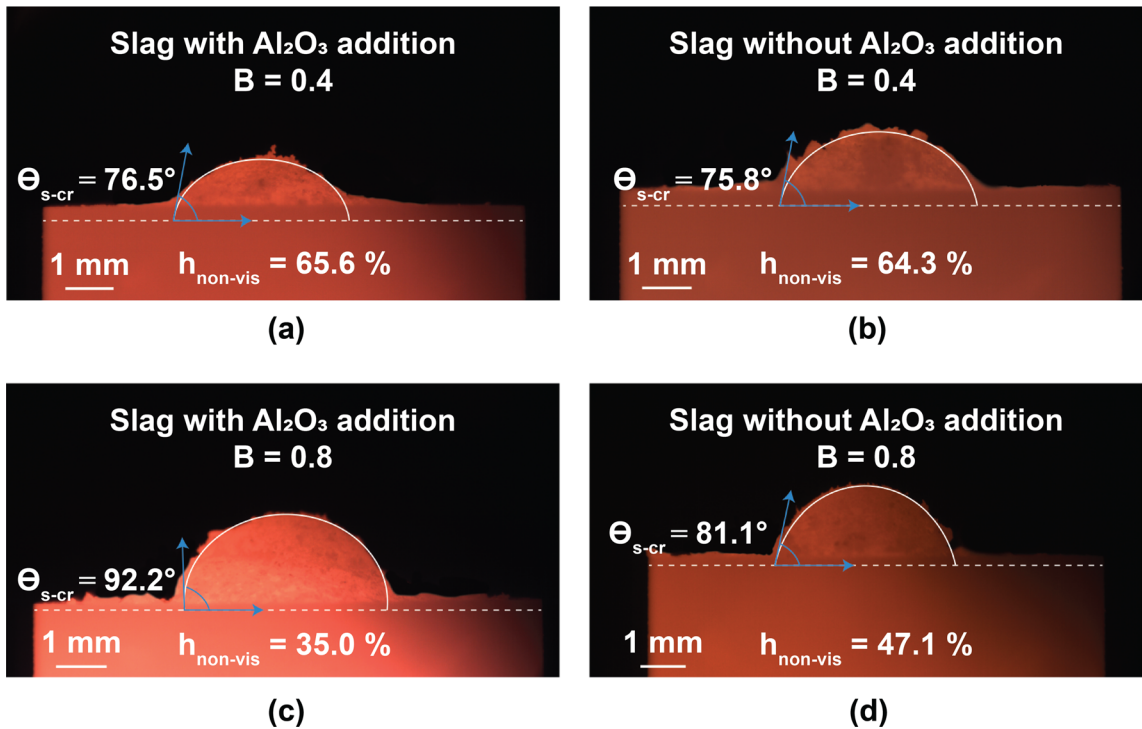As illustrated in Figure 11, the variation in MnO content in the slag from 30.0 to 45.0 wt pct at basicity of 0.8 shows that both the non-visible height of the slag droplet and the angle between slag and the top of the crucible are nearly constant which results in comparable values of the interfacial tension for all MnO contents. Similarly, the addition of Al_2O_3 to the low basicity slag (Figures 12(a) and (b)) does not show any influence on the non-visible height and the angle θ_{s-cr}, while the effect of alumina addition is more obvious at a higher slag basicity of 0.8 (Figures 12(c) and (d)) as the angle θ_{s-cr} decreases and the non-visible height increases which leads to lower values of the interfacial tension and therefore worse separation of slag and metal.

C. EPMA Results

A general view of the FeMn alloy and slags with and without Al_2O_3 addition after the experiments in the sessile drop furnace is shown in Figures 13 and 14, respectively. As observed for the slags with low basicities (0.4 and 0.8), the slag penetrates the FeMn phase, indicating that the interface is disturbed and the interfacial area increases due to the chemical reactions between the slag and metal. The chemical composition of slag and metal phases (Tables VIII and IX in "Appendix B") confirms that interfacial tension decreases at low slag basicity due to chemical reactions between slag and FeMn alloy and mass transfer of Si to the metal phase. As such, Si can be found in the metal phases after interaction with the low basicity slags at high temperatures, despite the fact that Si was not originally added to the FeMn alloy, which indicates that SiO_2 in the slag is reduced through Reaction (2). In addition, FeMn droplets were observed on top of the slag phase (Figures 13(a) and 14(a)), specifying that the slag of low basicity and the FeMn alloy form a metal–slag emulsion during the reactions, resulting in their poor separation.

Chung and Cramb[12] suggested that the emulsification phenomena are closely related to the interaction of fluids at the interface and that the driving force for fluid flow across the interface depends on reactions in the system under isothermal conditions due to the concentration gradient at the interface. In case of the concentration gradient and the fluid flow driven by the

Fig. 13—BSE images of the FeMn alloy and slags with Al_2O_3 addition after the experiments: (a) slag B1 (basicity = 0.4), (b) slag B2 (basicity = 0.8), and (c) slag B3 (basicity = 1.2).

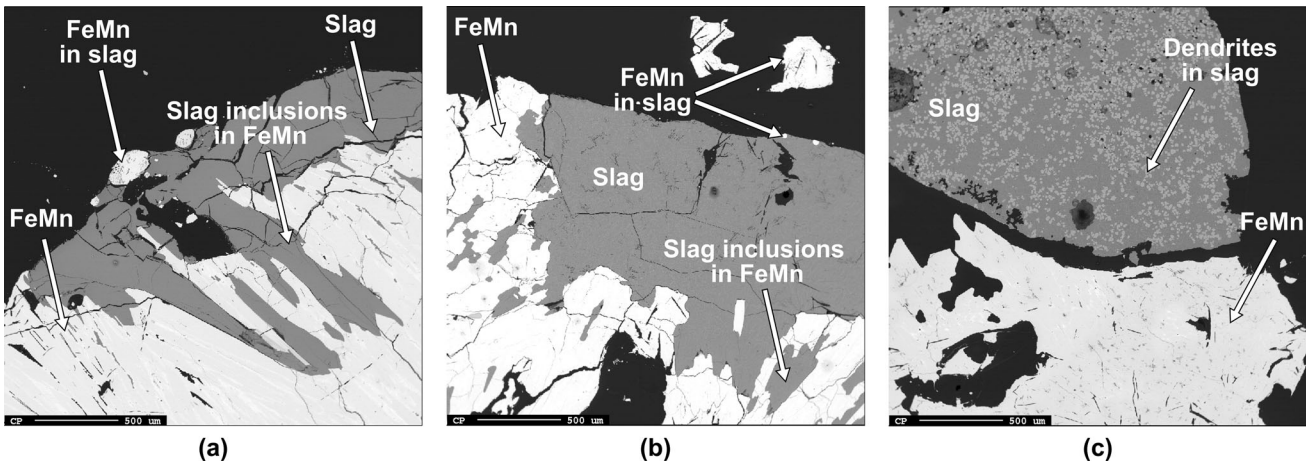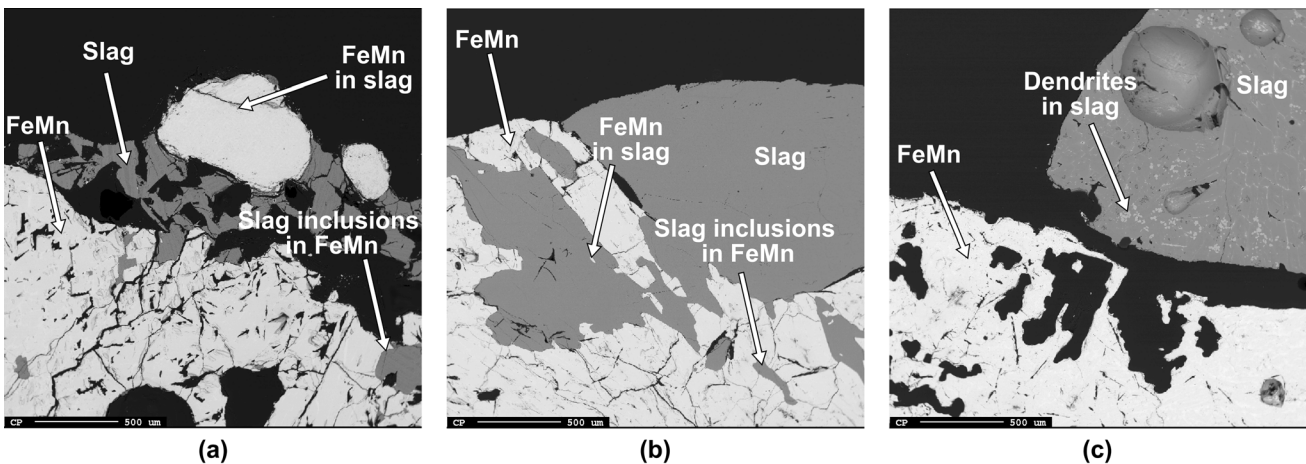Fig. 14—BSE images of the FeMn alloy and slags without Al_2O_3 addition after the experiments: (a) slag E1 (basicity = 0.4), (b) slag E2 (basicity = 0.8), and (c) slag E3 (basicity = 1.2).

interfacial reaction, the interface eventually becomes unstable and the metal–slag interfacial area increases (the Kelvin–Helmholtz interfacial instability). Based on the Kelvin–Helmholtz model, Gopal[3] discussed the mechanism of small droplet formation and emulsification of slag and metal during reactions between them. If the mass transfer rate of elements or compounds across the interface is low, it results in a slight destabilization of the interface (Figure 15(a)), corresponding to the high slag basicity of 1.2 in this study. At higher mass transfer rates, the destabilization of the interface is more severe as shown in Figures 15(b) and (c), which results in the
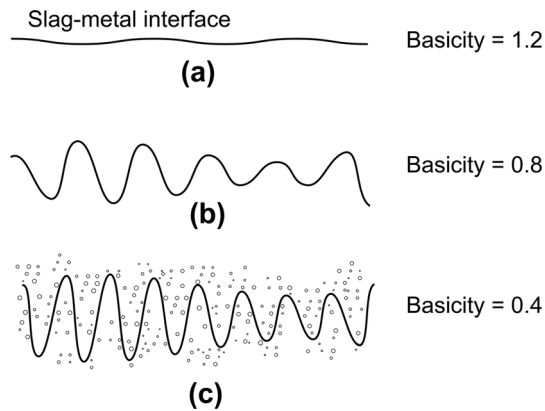

Fig. 15—Emulsification of slag and metal and formation of small droplets due to the Kelvin–Helmholtz instability. Images (*a*) through (*c*) represent disturbances of the interface between slag and metal at different slag basicities.

formation of the metal–slag emulsion and droplets of one phase into another as it was observed for the low slag basicities from 0.4 to 0.8.

Solid carbon particles in the form of graphite whiskers have been observed on top of FeMn layer and along the walls of the graphite cup in all experiments as illustrated in Figure 16. The formation of the solid carbon particles may be attributed to different temperatures used for the materials preparation and the experiments.[24] Bao *et al.*[32] also confirmed this finding and showed that solid carbon particles can form extensively when non-carbon saturated FeMn alloy reacts with slag and a graphite substrate, especially if CO is present in the system. In addition, carbon is consumed from the FeMn alloy due to the partial reduction of MnO, SiO_2 and FeO by Reactions (1), (2) and (3), therefore this creates an additional driving force for the FeMn alloy to dissolve carbon from the graphite cup, which causes the molten FeMn alloy to penetrate the walls of the graphite cup.

IV. CONCLUSIONS

In the present study, the interaction between FeMn alloy and slags of different compositions has been studied by comparing experimental results from a sessile drop furnace and modelling results from multiphase flow simulations in OpenFOAM.

The current results show that the interfacial tension between FeMn alloy and slag increases when the slag basicity changes from 0.4 to 1.2. It was also found that the addition of Al_2O_3 to the slag with basicity of 0.8 and
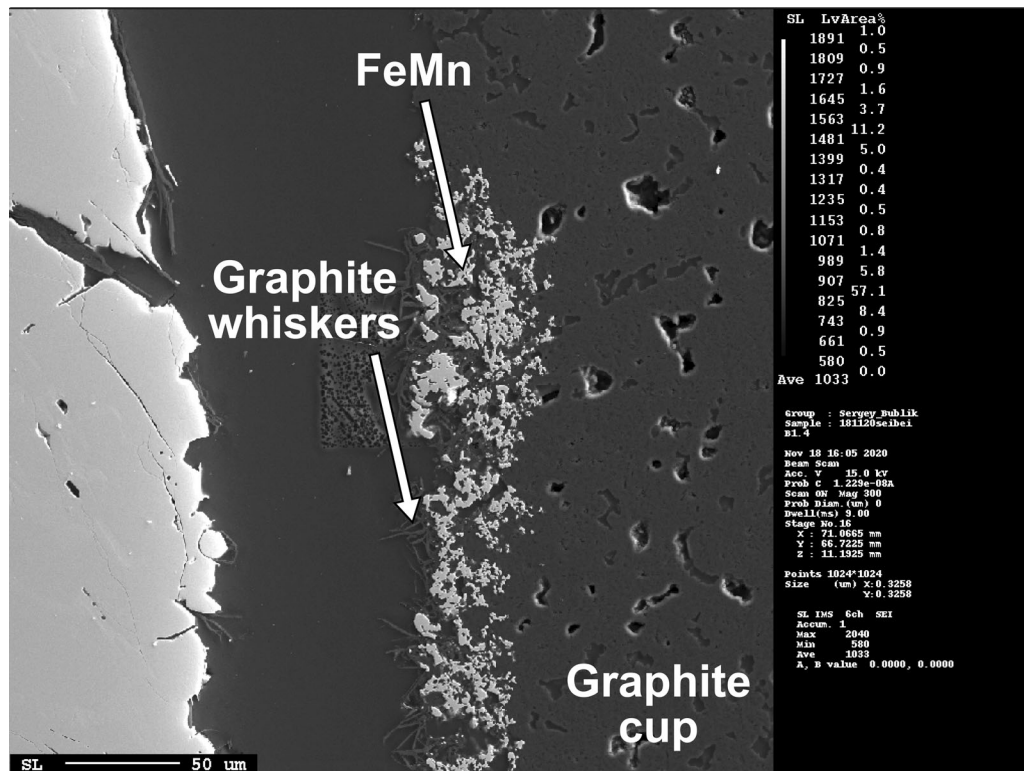

Fig. 16—FeMn alloy inclusions in the graphite cup and graphite whiskers formed along the walls of the graphite cup.

1.2 increases the interfacial tension, while increasing MnO content from 30.0 to 45.0 wt pct does not have any statistically significant influence on the interfacial tension.

EPMA analysis demonstrates an important phenomenon which contributes to the understanding of interfacial tension drop at low slag basicity. SiO_2 in the slag is reduced by the saturated carbon from the FeMn alloy at the interface and afterwards Si distributes to the metal phase. The mass transfer of Si across the interface creates the interface instability due to the growing interfacial area between slag and FeMn, which leads to the formation of a metal–slag emulsion and small droplets and, thus, to an increase in losses of the FeMn alloy with the slag.

Since the study was limited to using only graphite crucibles for the materials preparation and graphite cups for the melting experiments in the sessile drop furnace, solid carbon particles were observed on the surface of the slag and the FeMn alloy in the experiments, which may introduce additional uncertainty to the experimental results. However, the surface roughness correction coefficient has been used in this study to address this issue.

Further experiments, using a broader range of MnO content in the slag, could provide more data on the effect of MnO influence on the interfacial tension between slag and metal, which might be crucial for the ferroalloy industry. In addition, experiments in the sessile drop furnace with cups made of different materials can be a further development of the current methodology.

CONFLICT OF INTEREST

On behalf of all authors, the corresponding author states that there is no conflict of interest.

APPENDIX A

See Tables IV, V, VI and VII.

Table IV. The Calculated Chemical Composition of the Synthetic FeMn Alloy and Slags

Material	Chemical Composition (Wt Pct)								
	Mn	Fe	C	MnO	CaO	MgO	SiO_2	Al_2O_3	Basicity
FeMn Alloy	78.00	15.00	7.00	—	—	—	—	—	—
Slags with Al_2O_3 Addition									
Master Slag #1	—	—	—	38.00	23.00	6.00	23.00	10.00	0.9
Slag A1	—	—	—	30.00	14.00	6.00	40.00	10.00	0.4
Slag A2	—	—	—	30.00	25.11	6.00	28.89	10.00	0.8
Slag A3	—	—	—	30.00	32.18	6.00	21.82	10.00	1.2
Slag B1	—	—	—	37.50	11.86	6.00	34.64	10.00	0.4
Slag B2	—	—	—	37.50	21.78	6.00	24.72	10.00	0.8
Slag B3	—	—	—	37.50	28.09	6.00	18.41	10.00	1.2
Slag C1	—	—	—	45.00	9.71	6.00	29.29	10.00	0.4
Slag C2	—	—	—	45.00	18.44	6.00	20.56	10.00	0.8
Slag C3	—	—	—	45.00	24.00	6.00	15.00	10.00	1.2
Slags Without Al_2O_3 Addition									
Master Slag #2	—	—	—	42.52	25.74	6.00	25.74	—	1.2
Slag D1	—	—	—	30.00	14.00	6.00	50.00	—	0.4
Slag D2	—	—	—	30.00	25.11	6.00	38.89	—	0.8
Slag D3	—	—	—	30.00	32.18	6.00	31.82	—	1.2
Slag E1	—	—	—	37.50	11.86	6.00	44.64	—	0.4
Slag E2	—	—	—	37.50	21.78	6.00	34.72	—	0.8
Slag E3	—	—	—	37.50	28.09	6.00	28.41	—	1.2
Slag F1	—	—	—	45.00	9.71	6.00	39.29	—	0.4
Slag F2	—	—	—	45.00	18.44	6.00	30.56	—	0.8
Slag F3	—	—	—	45.00	24.00	6.00	25.00	—	1.2

Table V. The Purity of the Powders Used for the Preparation of the Synthetic Raw Materials

			Purity of Corresponding Powders (Pct)			
Mn	Fe	MnO	CaO	MgO	SiO$_2$	Al$_2$O$_3$
99.30	99.00	99.00	95.00	99.00	99.50	99.00

Table VI. Normalized Values of the Measured Chemical Composition of the Synthetic FeMn Alloy and Slags

					Chemical Composition (Wt Pct)							
Material	Mn	Fe	Si	C	MnO	CaO	MgO	SiO$_2$	Al$_2$O$_3$	FeO	Total	Basicity
FeMn Alloy	77.75	14.58	0.11	7.56	—	—	—	—	—	—	100.00	—
Slags with Al$_2$O$_3$ Addition												
Slag A1	—	—	—	—	29.94	13.92	6.62	38.65	10.00	0.87	100.00	0.42
Slag A2	—	—	—	—	28.81	25.08	6.64	28.70	10.00	0.78	100.00	0.82
Slag A3	—	—	—	—	28.72	31.79	6.60	21.99	10.12	0.78	100.00	1.20
Slag B1	—	—	—	—	36.94	12.55	6.55	33.29	9.92	0.75	100.00	0.44
Slag B2	—	—	—	—	36.09	22.08	6.46	24.74	9.89	0.73	100.00	0.82
Slag B3	—	—	—	—	37.04	27.51	6.74	18.09	9.88	0.73	100.00	1.22
Slag C1	—	—	—	—	44.28	10.49	6.44	28.11	9.97	0.71	100.00	0.44
Slag C2	—	—	—	—	43.67	18.62	6.68	20.34	9.97	0.71	100.00	0.83
Slag C3	—	—	—	—	44.60	23.50	6.58	14.78	9.83	0.71	100.00	1.22
Slags Without Al$_2$O$_3$ Addition												
Slag D1	—	—	—	—	30.09	14.48	5.99	47.91	0.66	0.87	100.00	0.42
Slag D2	—	—	—	—	29.42	24.96	6.22	37.80	0.76	0.84	100.00	0.81
Slag D3	—	—	—	—	28.98	31.59	6.12	31.91	0.60	0.79	100.00	1.16
Slag E1	—	—	—	—	37.78	12.63	5.95	42.32	0.57	0.75	100.00	0.43
Slag E2	—	—	—	—	36.39	22.31	6.06	33.82	0.68	0.74	100.00	0.82
Slag E3	—	—	—	—	36.81	27.85	6.03	28.03	0.67	0.60	100.00	1.18
Slag F1	—	—	—	—	44.94	10.34	6.09	37.26	0.67	0.69	100.00	0.43
Slag F2	—	—	—	—	43.53	19.29	5.99	29.98	0.55	0.67	100.00	0.83
Slag F3	—	—	—	—	44.42	24.03	5.89	24.51	0.46	0.69	100.00	1.20

Table VII. Weight of the Powders Used for the Preparation of the Synthetic Raw Materials

			Weight of Powders (g)					
Material	Mn	Fe	MnO	CaO	MgO	SiO$_2$	Al$_2$O$_3$	Total
FeMn	211.16	40.73	—	—	—	—	—	251.89
Slags with Al$_2$O$_3$ Addition								
Master Slag #1	—	—	95.00	57.50	15.00	57.50	25.00	250.00
Powders Addition to Master Slag #1, g								
Slag A1	—	—	2.28	—	0.78	8.59	1.30	12.95
Slag A2	—	—	—	1.85	0.32	2.73	0.54	5.44
Slag A3	—	—	—	3.74	0.32	0.93	0.54	5.53
Slag B1	—	—	7.02	—	1.14	8.88	1.90	18.94
Slag B2	—	—	0.32	—	0.07	0.63	0.11	1.13
Slag B3	—	—	1.79	2.55	0.30	—	0.50	5.14
Slag C1	—	—	13.85	—	1.66	9.31	2.76	27.58
Slag C2	—	—	3.66	—	0.30	0.53	0.50	4.99
Slag C3	—	—	6.26	2.91	0.65	—	1.08	10.90
Slags Without Al$_2$O$_3$ Addition								
Master Slag #2	—	—	106	64	15	64	—	250.00
Powders Addition to Master Slag #2, g								
Slag D1	—	—	3.47	0.58	1.02	13.85	—	18.92
Slag D2	—	—	0.91	2.65	0.51	6.46	—	10.53
Slag D3	—	—	0.91	4.76	0.51	4.44	—	10.62
Slag E1	—	—	8.77	0.58	1.42	14.86	—	25.63

Table VII. continued

Material	Mn	Fe	MnO	CaO	MgO	SiO$_2$	Al$_2$O$_3$	Total
				Weight of Powders (g)				
Slag E2	—	—	1.28	0.58	0.22	3.63	—	5.71
Slag E3	—	—	0.91	1.86	0.16	1.85	—	4.78
Slag F1	—	—	16.41	0.58	2.00	16.30	—	35.29
Slag F2	—	—	5.01	0.58	0.48	3.95	—	10.02
Slag F3	—	—	2.07	0.58	0.09	0.77	—	3.51

APPENDIX B

See Tables VIII and IX.

Table VIII. Average Chemical Composition (in Wt Pct) of Slag Phases after the Experiments in the Sessile Drop Furnace

Slag	Matrix*	Dendrites*	MnO	CaO	MgO	SiO$_2$	Al$_2$O$_3$	FeO	Total
Bulk									
B1	100	—	28.85	16.23	8.01	33.35	13.35	0.09	99.89
B2	100	—	27.30	25.78	7.36	27.01	12.72	0.06	100.21
B3	82	18	30.20	30.36	6.43	19.77	13.11	0.08	99.95
E1	70/30**	—	40.86	13.58	8.44	36.54	0.46	0.10	99.98
E2	87/13**	—	34.79	22.51	7.15	34.36	0.54	0.10	99.45
E3	87	13	33.65	28.13	7.97	29.53	0.05	0.09	99.43
Slag Inclusions in the Metal Phase									
B1	100	—	32.41	14.88	7.59	32.87	12.21	0.15	100.11
B2	100	—	27.94	25.38	7.24	27.02	13.02	0.40	101.00
B3	—	—	—	—	—	—	—	—	—
E1	70/30**	—	37.94	13.84	9.95	37.41	0.64	0.18	99.96
E2	87/13**	—	35.26	22.52	6.91	33.17	0.77	0.20	98.82
E3	—	—	—	—	—	—	—	—	—

*Percentage from the total surface area of the slag phase.
**Matrix consists of two distinctive phases: bright and grey.

Table IX. Average Chemical Composition (in Wt Pct) of the FeMn Alloy After the Experiments in the Sessile Drop Furnace

Slag in experiment	Phase	Mn	Fe	Si	C	Total
Bulk						
B1	Bright	75.90	19.23	0.57	5.07	100.78
	Grey	79.23	13.61	0.00	6.12	98.96
	Dark	79.46	13.69	2.78	5.18	101.11
B2	Bright	75.61	19.57	0.12	4.69	99.98
	Dark	79.39	13.53	0.00	5.87	98.79
B3	Bright	73.79	22.66	0.10	5.19	101.75
	Grey	75.74	19.15	0.00	6.19	101.08
	Dark	78.78	14.30	0.00	6.96	100.04
E1	Bright	67.95	26.10	3.95	4.59	102.58
	Grey	72.79	21.00	1.28	5.73	100.80
	Dark	79.08	14.66	0.00	5.80	99.55
E2	Grey	79.96	13.76	0.01	6.49	100.23
E3	Bright	72.51	27.54	0.32	4.11	104.48
	Grey	77.66	17.54	0.00	5.62	100.82
	Dark	80.19	13.63	0.00	6.08	99.89
Near the Interface						
B1	Bright	72.36	22.12	2.32	4.43	101.22
	Dark	80.25	13.35	0.01	6.22	99.83

Table IX. continued

Slag in experiment	Phase	Mn	Fe	Si	C	Total
B2	Bright	75.57	23.56	0.13	2.98	102.24
	Grey	79.59	15.31	0.00	5.16	100.06
	Dark	79.74	13.81	0.00	5.75	99.30
B3	Bright	74.52	23.03	0.03	4.64	102.22
	Grey	76.77	17.88	0.00	6.22	100.87
	Dark	79.40	13.85	0.00	6.83	100.08
E1	Bright	73.13	20.09	4.50	4.87	102.58
	Dark	81.68	11.76	0.03	5.92	99.39
E2	Bright	77.25	17.81	0.01	6.00	101.07
	Grey	79.71	14.15	0.00	6.63	100.50
E3	Bright	74.56	23.87	0.19	3.80	102.42
	Grey	76.59	19.20	0.02	5.76	101.56
	Dark	79.89	13.41	0.00	6.42	99.72
FeMn Inclusions in the Graphite Cup						
B1	Bright	77.17	14.82	0.02	8.08	100.08
B2	Bright	75.93	14.81	0.00	7.67	98.42
B3	Bright	76.42	14.18	0.00	8.99	99.60
E1	Bright	77.32	13.83	0.00	7.32	98.48
E2	Bright	76.79	14.89	0.00	8.10	99.79
E3	Bright	73.84	14.60	0.03	9.48	97.94

REFERENCES

1. M. Tangstad: *Handbook of Ferroalloys*, Butterworth-Heinemann, Oxford, 2013.
2. R.H. Eric: *Treatise on Process Metallurgy*, Elsevier, Boston, 2014, pp. 477–532.
3. E.S.R. Gopal: *Principles of Emulsion Formation*, Academic, London, 1968, pp. 1–75.
4. P.R. Scheller, J. Lee, and T. Tanaka: *Treatise on Process Metallurgy*, Elsevier, Boston, 2014, pp. 111–18.
5. P. Ni, T. Tanaka, M. Suzuki, M. Nakamoto, and P.G. Jönsson: *ISIJ Int.*, 2019, vol. 59, pp. 737–48.
6. E.-J. Jung, W. Kim, I. Sohn, and D.-J. Min: *J. Mater. Sci.*, 2010, vol. 45, pp. 2023–29.
7. S.-C. Park, H. Gaye, and H.-G. Lee: *Ironmak. Steelmak.*, 2009, vol. 36, pp. 3–11 .
8. T. Tanaka, H. Goto, M. Nakamoto, M. Suzuki, M. Hanao, M. Zeze, H. Yamamura, and T. Yoshikawa: *ISIJ Int.*, 2016, vol. 56, pp. 944–52.
9. L. Muhmood, N.N. Viswanathan, and S. Seetharaman: *Metall. Mater. Trans. B*, 2011, vol. 42B, pp. 460–70.
10. H. Sun, K. Nakashima, and K. Mori: *ISIJ Int.*, 2006, vol. 46, pp. 407–12.
11. K. Nakashima and K. Mori: *ISIJ Int.*, 1992, vol. 32, pp. 11–18.
12. Y. Chung and A.W. Cramb: *Metall. Mater. Trans. B*, 2000, vol. 31B, pp. 957–71.
13. Y.E. Lee and L. Kolbeinsen: *Metall. Mater. Trans. B*, 2021, vol. 52, pp. 3142–3150.
14. A. Jakobsson, D. Sichen, S. Seetharaman, and N.N. Viswanathan: *Metall. Mater. Trans. B*, 2000, vol. 31B, pp. 973–80.
15. H. Terasaki, S. Urakawa, K. Funakoshi, N. Nishiyama, Y. Wang, K. Nishida, T. Sakamaki, A. Suzuki, and E. Ohtani: *Phys. Earth Planet. Inter.*, 2009, vol. 174, pp. 220–26.
16. S. Bublik, S. Bao, M. Tangstad, and K.E. Einarsrud: *Proc. Liq. Met. Process. Cast. Conf. (2019)*, Birmingham, UK, 2019, pp. 375–84.
17. S. Bublik and K.E. Einarsrud: *14th International Conference on CFD in Oil and Gas, Metallurgical and Process Industries*, Trondheim, Norway, SINTEF Academic Press, 2020, pp. 28–38.
18. H.G. Weller, G. Tabor, H. Jasak, and C. Fureby: *Comput. Phys.*, 1998, vol. 12, pp. 620–31.
19. K.C. Mills, Y. Lang, and R.T. Jones: *J. S. Afr. Inst. Min. Metall.*, 2011, vol. 111, pp. 649–58.
20. K.C. Mills, S. Karagadde, P.D. Lee, L. Yuan, and F. Shahbazian: *ISIJ Int.*, 2016, vol. 56, pp. 264–73.
21. C.W. Bale, E. Bélisle, P. Chartrand, S.A. Decterov, G. Eriksson, A.E. Gheribi, K. Hack, I.H. Jung, Y.B. Kang, J. Melançon, A.D. Pelton, S. Petersen, C. Robelin, J. Sangster, P. Spencer, and M.-A. Van Ende: *CALPHAD: Comput. Coupling Phase Diagr. Thermochem.*, 2016, vol. 54, pp. 35–53.
22. S. Bao, K. Tang, A. Kvithyld, M. Tangstad, and T.A. Engh: *Metall. Mater. Trans. B*, 2011, vol. 42B, pp. 1358–66.
23. J. Muller, J.H. Zietsman, and P.C. Pistorius: *Metall. Mater. Trans. B*, 2015, vol. 46B, pp. 2639–51.
24. S. Bublik, S. Bao, M. Tangstad, and K.E. Einarsrud: *Metall. Mater. Trans. B*, 2021, vol. 52B, pp. 3624–45.
25. D.C. Montgomery: *Design and Analysis of Experiments*, 8th ed., Wiley, Hoboken, NJ, 2013.
26. P. Patnaik: *Handbook of Inorganic Chemicals*, McGraw-Hill, New York, 2003.
27. P. Ni, T. Tanaka, M. Suzuki, M. Nakamoto, and P.G. Jönsson: *ISIJ Int.*, 2018, vol. 58, pp. 1979–88.
28. K. Gu, N. Dogan, and K.S. Coley: *Metall. Mater. Trans. B*, 2017, vol. 48B, pp. 2595–2606.
29. H. Sun, K. Nakashima, and K. Mori: *ISIJ Int.*, 1997, vol. 37, pp. 323–31.
30. S. Rosypalova, R. Dudek, and J. Dobrovska: *Proc. 21st Int. Metall. Mater. Conf.*, Ostrava, 2012, pp. 109–14.
31. S. Rosypalova, R. Dudek, J. Dobrovska, L. Dobrovsky, and M. Zaludova: *Mater. Technol.*, 2014, vol. 48, pp. 415–18.
32. S. Bao, M. Tangstad, K. Tang, K.E. Einarsrud, M. Syvertsen, M. Onsøien, A. Kudyba, and S. Bublik: *Metall. Mater. Trans. B*, 2021, vol. 52B, pp. 2847–58.